# GPM Combined Radar-Radiometer Precipitation Algorithm Theoretical Basis Document (Draft 1)

Willam S. Olson, Hirohiko Masunaga

and the

GPM Combined Radar-Radiometer Algorithm Team

November 23, 2010

**Table of Contents**

## 1. Introduction

The GPM Combined Radar-Radiometer Algorithm performs two basic functions: first, it provides, in principle, the most accurate, high resolution estimates of surface rainfall rate and precipitation vertical precipitation distributions that can be achieved from a spaceborne platform, and it is therefore valuable for applications where information regarding instantaneous storm structure are vital. Second, long-term accumulation of combined algorithm estimates will yield a single common reference dataset that will be used to "cross-calibrate" rain rate estimates from all of the passive microwave radiometers in the GPM constellation. The cross-calibration of the radiometer estimates is crucial for developing a consistent, high-time-resolution precipitation record for climate science and prediction model validation applications. Because of the Combined Algorithm's essential roles as accurate reference and calibrator, the GPM Project is supporting a Combined Algorithm Team to implement and test the algorithm prior to launch. In the pre-launch phase, GPM-funded science investigations may lead to significant improvements in algorithm function, but the basic algorithm architecture has been formulated. This algorithm architecture is largely consistent with the successful TRMM Combined Algorithm design, but it has been updated and modularized to take advantage of improvements in the representation of physics, new climatological background information, and model-based analyses that may become available at any stage of the mission. This document presents a description of the GPM Combined Algorithm architecture, scientific basis, inputs/outputs, and supporting ancillary datasets.

## 2. Background

*GPM Instruments*

The GPM core mission satellite observatory is shown in Fig. 1. From this platform, the Dual-frequency Precipitation Radar (DPR) scans cross-track in relatively narrow swaths at Ku band (13.6 GHz) and Ka band (35.5 GHz). The dual-frequency radar reflectivity observations are nearly beam-matched over the 125 km Ka-band swath, with a horizontal resolution of approximately 5 km, and a vertical resolution of 250 m in standard observing mode. The Ku-band radar scans over a wider, 245 km swath. The GPM Microwave Imager (GMI) scans conically over an 885 km wide swath at frequencies of 10.7, 18.7, 23.8, 89.0, 165.5, 183.3 ± 7, and 183.3 ± 3 GHz. Measured brightness temperatures are in two polarizations (vertical and horizontal) at all but the 23.8 GHz and 183.3 GHz channels, which provide only vertical polarization measurements. The GMI observations are diffraction limited, with the lowest-resolution footprints (approx. 26 km) at 10.7 GHz and the highest-resolution footprints (approx. 6 km) at the 89.0 GHz and higher frequency channels.

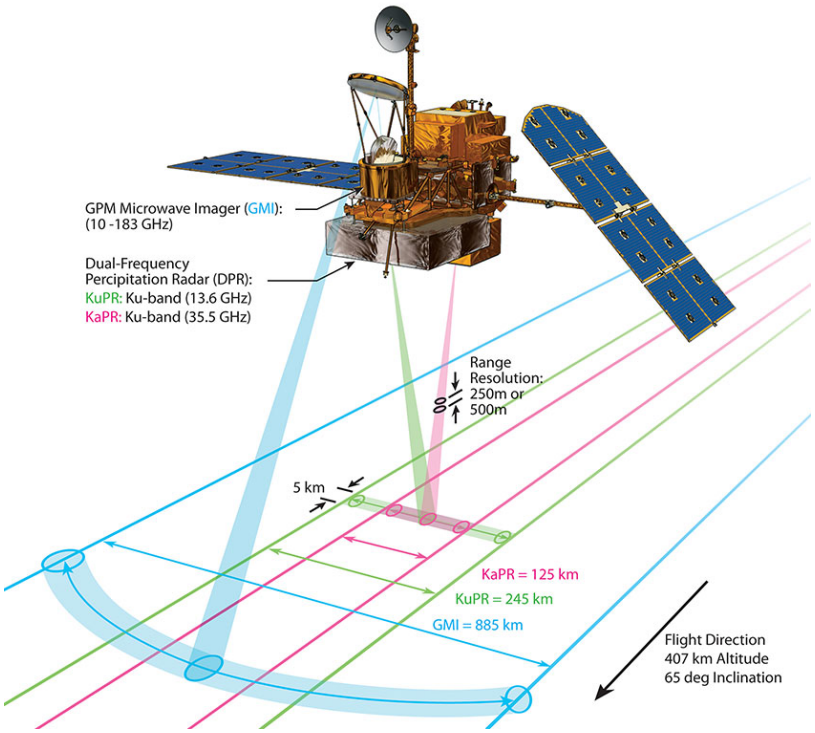


Fig. 1. Configuration of the GPM core observatory, showing the scanning by the DPR and GMI instruments.

*Implications for Algorithm Design*

The current GPM Combined Radar-Radiometer Algorithm architecture derives from a rich heritage of algorithms that were developed for the TRMM mission, as well as other algorithms developed and applied to airborne radar-radiometer data. In TRMM, only Ku-band radar observations were available from the radar instrument ( the Precipitation Radar, or PR), and only lower-frequency ($\leq$ 85 GHz) brightness temperature measurements were available from the microwave radiometer (the TRMM Microwave Imager, or TMI). The TRMM Facility Combined Algorithm used radiometer information to essentially reduce uncertainties in estimates of radar-derived total path-integrated attenuation to the earth's surface to perform an improved attenuation correction of the vertical radar profile. The improved attenuation correction was effected by adjusting a single parameter of the precipitation particle-size distribution over the entire vertical precipitation profile. This single parameter represented a rain-normalized, mass-weighted mean particle diameter, which was assumed to be locally constant over the scale of TMI footprints because adding horizontal variations would have introduced too many degrees of freedom in the inversion problem.

The GPM Combined Algorithm takes advantage of the additional information provided by the Ka-band radar channel to glean more specific information about the precipitation size distribution and associated attenuation in each gate. This estimation of precipitation size distribution parameters is aided by precipitation attenuation information from the GMI channels, which have an extended spectral

range relative to the TMI. However, if the Ka-band reflectivities do not provide additional information due to very light rain (Rayleigh limit), or they are severely attenuated in heavy precipitation, then the combined algorithm must make a natural transition to a single-frequency, Ku-band solution in which a more approximate estimation of precipitation size distribution parameters is performed.

Regardless of whether or not the Ka-band data are applicable, however, information from the GMI brightness temperatures can be used to make further adjustments of path attenuation due to non-precipitating cloud liquid water and water vapor, which are not directly sensed by the DPR. In addition, there are other microphysical parameters, such as the degree of non-exponentiality of the precipitation size distribution and the density of ice-phase precipitation that may be adjusted using radiometer information.

Ultimately, the degree to which any precipitation or environmental parameters can be adjusted is limited by the information content of the DPR and GMI observations and any additional information provided by *a priori* data, such as the natural ranges of particle size distribution parameters, cloud water contents, etc., and how these parameters covary spatially. Therefore, as outlined in Section 3, the combined algorithm is designed to be able to accept both different physical modeling assumptions and *a priori* constraints on estimated parameters.

## 3. Algorithm Architecture

*Overview*

The current algorithm design is based upon a hybrid ensemble Kalman filtering (EnKF)/variational approach for inverting the DPR reflectivities and GMI brightness temperatures to estimates precipitation profiles. Because the EnKF method is applied multiple times in the algorithm, a brief description of the method, in 1-D, is provided here; the variational method will be described later in this section. Given an observation $y_{obs}$, an unknown parameter $x$, and a presumed forward model $y(x)$, the EnKF method is used to estimate an ensemble of $x$ values that are consistent with the observation and its uncertainty, $\sigma_{yobs}$. First, given an assumed *a priori* distribution of $x$, an ensemble of $x_i$ values is selected at random. Usually an ensemble of 50 members is sufficient to represent the statistics of $x$ in the method. The forward model $y(x)$ is then used to calculate an ensemble of $y_i$ values corresponding to the ensemble of $x_i$ values. The ensemble $x_i$ is then updated using

$$x_i' = x_i + \frac{\mathrm{cov}(x,y)}{\left(\mathrm{cov}(y,y) + \sigma_{yobs}^2\right)}\left(y_{obs} - y_i\right) \quad (1)$$

where cov() represents the covariance of the ensembles of variables within the parentheses. The updated ensemble $x_i'$ is consistent with the observation $y_{obs}$ and its uncertainty. The mean of the ensemble is the best estimate of $x$, and the standard deviation of the ensemble relative to the mean yields an estimate of the uncertainty of

*x*. The generalization of (1) to multiple observations and multiple unknowns is straightforward; see Anderson (2003).

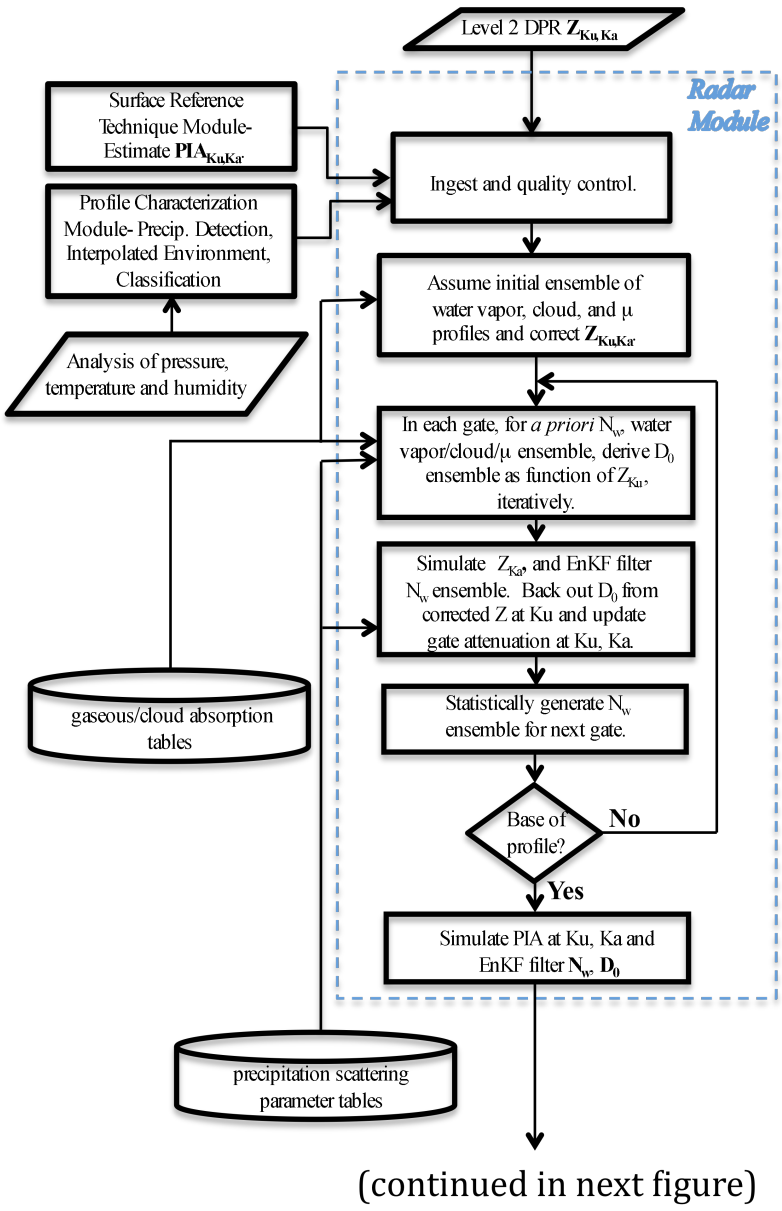


*Fig. 2a. Radar Module processing schematic of the Combined Radar-Radiometer Algorithm.*

The general architecture of the GPM Combined Algorithm is illustrated in Fig. 2. DPR reflectivities and total path-integrated attenuation estimates at Ku and Ka bands are first ingested by a Radar Module. The path-integrated attenuation estimates are determined using the Surface Reference Technique (SRT) in a Module developed by the GPM Radar Algorithm Team. Information concerning the general characteristics of the precipitation (precipitation detection, existence of a bright band, bright band altitude, convective/stratiform classification) and its environment (temperature and

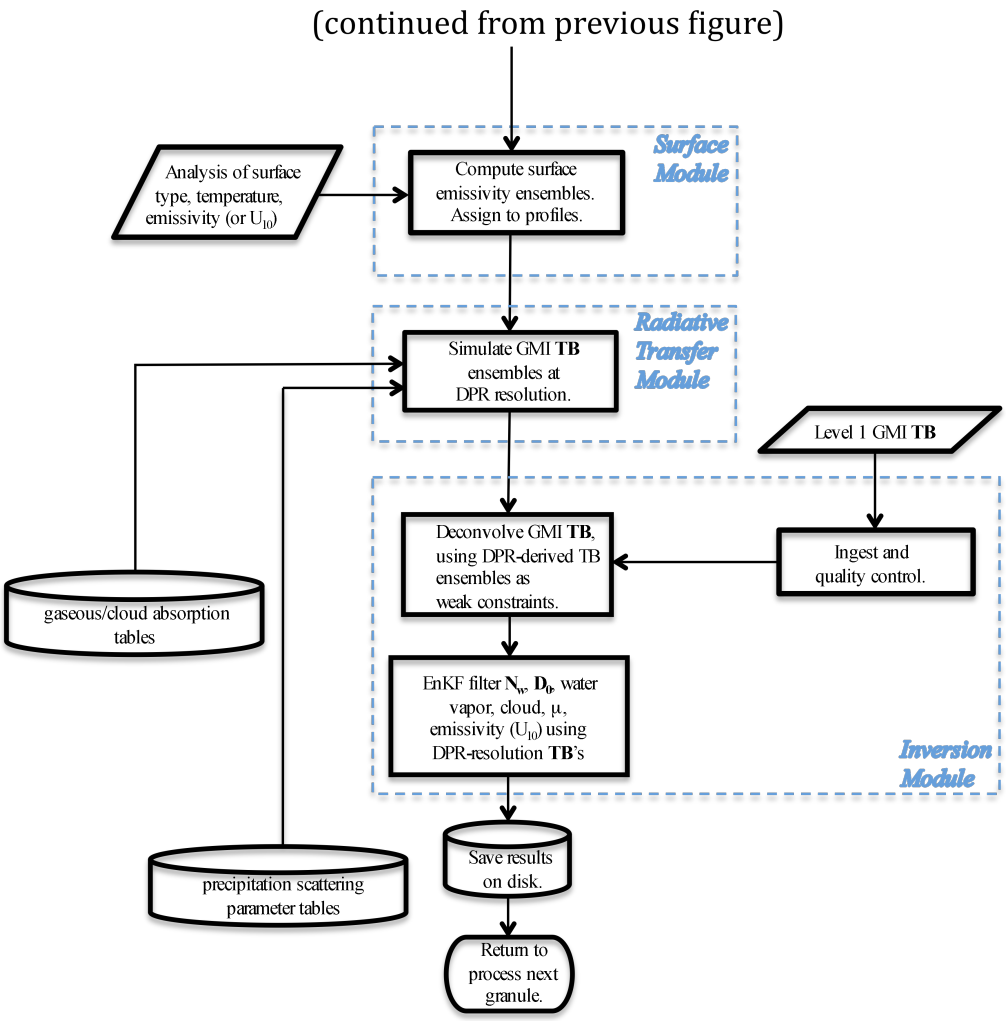


*Fig. 2b. Surface, Radiative Transfer, and Inversion Module processing schematic of the Combined Radar-Radiometer Algorithm.*

water vapor profiles) are supplied by a Profile Characterization Module, also supplied by the GPM Radar Team. After quality control of these data, initial *a priori* ensembles of temperature/water vapor profiles are randomly generated, based upon initial estimates from the Profile Characterization Module and their uncertainties. An ensemble of ~50 profile members is generated for each DPR footprint. To each profile member, a cloud liquid/ice profile is randomly assigned, based upon a distribution of cloud-system resolving model simulated profiles consistent with the environment at the DPR footprint location.

The initial temperature/water vapor/cloud water profiles are used to perform an initial attenuation correction of the Ku- and Ka-band reflectivities to create an ensemble of corrected reflectivity profiles. The attenuation by water vapor and cloud water in each profile is derived from tables of pre-calculated absorption coefficients, interpolated to the pressures, temperatures, humidities, and cloud liquid-equivalent

water contents in the given profile. The remaining attenuation in each member reflectivity profile is due to precipitation.

The estimation of precipitation size distribution parameters, and the associated radar reflectivities and attenuation due to precipitation, is based upon an assumed normalized gamma distribution of precipitation particle sizes.

$$n(D) = N_w \, f(\mu) \left( \frac{D}{D_o} \right)^{\mu} \exp\left( -\frac{(3.67 + \mu)}{D_o} D \right), \tag{2}$$

where

$$f(\mu) \;=\; \frac{6(3.67 + \mu)^{\mu+4}}{3.67^4 \, \Gamma(\mu + 4)} \,. \tag{3}$$

Here, $N_w$ is the intercept of the normalized distribution, $D_o$ is the median volume diameter, $\mu$ is the distribution shape factor, $D$ is the liquid-water equivalent diameter of the particle, and $n(D)$ is the spectral number density of particles with diameter $D$. In the Radar Module, $\mu$ values are randomly assigned to each radar profile ensemble member, based upon an *a priori* distribution. This leaves $N_w$ and $D_o$ as two unknowns to be estimated in each range gate.

Starting with the top-most radar gate with detectible precipitation, estimates of $N_w$ are assigned at random from an *a priori* distribution to each ensemble member reflectivity profile. Given the value of $N_w$ and the Ku-band reflectivity, $Z_{Ku}$, associated with a particular ensemble member profile in the top-most gate, a value of $D_o$ can be determined iteratively from the radar equation, using theoretical values of extinction and reflectivity (for the assumed $\mu$ and precipitation particle composition) provided by supporting scattering parameter tables (see Fig. 2a). In this way, values of $D_o$ are estimated for each ensemble member profile in the top-most gate, and the resulting $N_w/D_o$ pairs are associated with attenuation-corrected reflectivities at Ku band that are consistent with the observed $Z_{Ku}$. The estimated values of $N_w$ and $D_o$ are then used to simulate the attenuated reflectivity at Ka-band, $Z_{Ka}$, for each ensemble member profile. The ensemble covariance of the $N_w$ and simulated $Z_{Ka}$ values, in combination with the observed $Z_{Ka}$, are then used to update the *a priori* $N_w$ estimates based upon ensemble Kalman filtering. Next, the updated $N_w$ and attenuation-corrected $Z_{Ku}$ are used to identify consistent $D_o$ values, based upon the scattering parameter tables. In short, the foregoing procedure determines an ensemble of $N_w/D_o$ pairs that are consistent with the observed Ku- and Ka-band reflectivities (and their uncertainties) in the top-most gate.

To process the next-lowest gate, *a priori* $N_w$ values for the next-lowest gate are generated based upon the $N_w$ estimates in the top-most gate using a statistical, auto-regressive model. The procedure applied to the top-most gate can then be repeated for the next-lowest gate, producing an ensemble of $N_w/D_o$ estimates consistent with

the observed $Z_{Ku}$ and $Z_{Ka}$ in that gate. In this way, working down a given DPR profile recursively, an ensemble of $N_w/D_o$ profiles is estimated.

After the entire DPR profile has been processed, each estimated $N_w/D_o$ profile in the ensemble is associated with total path-integrated attenuations at Ku and Ka band. However, these estimated path-integrated attenuation values might not be consistent with the independent path-integrated attenuations (and uncertainties) estimated using the SRT. Therefore, the covariances of the $N_w/D_o$ profiles and associated path-integrated attenuations, in combination with the SRT path-integrated attenuations, are used to update the member $N_w/D_o$ profiles based upon ensemble Kalman filtering. The resulting ensemble of $N_w/D_o$ profiles is consistent with the Ku- and Ka-band reflectivity profiles and SRT estimates of total path-integrated attenuation.

The foregoing procedure is applied to each DPR profile in the radar swath. If the Ka-band reflectivity data are not available or unusable (completely attenuated), then only the Ku-band data and the associated path-integrated attenuation from the SRT are utilized. In the Rayleigh limit (very light rain rates), the Ka-band data will not supply independent information and their impact on estimates of $N_w/D_o$ will be small.

After the DPR swath has been processed by the Radar Module, the ensembles of DPR-consistent $N_w/D_o$ profiles are then passed to the Surface Module (see Fig. 2b). Here, estimates of microwave surface emissivity at the GMI channel frequencies/polarizations are assigned at random to each ensemble member profile. Over water surfaces, an explicit model is used to calculate emissivities at all frequencies/polarizations as functions of surface skin temperature, salinity, and 10-meter wind speed. Estimates of surface skin temperature and 10-meter wind speed, as well as their uncertainties, are interpolated from an analysis to the DPR footprints in the Profile Characterization Module, and values of salinity and their variances are derived from a climatological database. Random generation of these inputs (within their uncertainties) to the emissivity model results in an ensemble of computed emissivities that are assigned to the ensemble of vertical profiles at each DPR footprint location. For land surfaces, there is no explicit model for surface emissivity, and so a satellite-derived climatology of emissivities and their covariances is used to randomly assign emissivities to each DPR-derived ensemble profile member.

The $N_w/D_o$ profile ensembles and assigned emissivities are next passed to the Radiative Transfer Module. This module computes the upwelling microwave brightness temperatures associated with each ensemble member profile at all of the GMI channel frequencies/polarizations. Currently, Eddington's Second Approximation is used to compute these upwelling brightness temperatures at the GMI viewing angle, assuming a plane-parallel atmosphere.

The $N_w/D_o$ profile ensembles and associated upwelling brightness temperatures are estimated at the DPR horizontal resolution and sampling (5 km). On the other hand, GMI brightness temperature observations have a horizontal resolution (footprint dimension) ranging from roughly 26 km at 10.7 GHz to 6 km at 183.3 GHz

due to the diffraction limitation of the sensor, and the sample spacing of GMI is approximately 6 km cross-track and 14 km along-track. The proposed mitigation of the relatively low resolution of the GMI is to deconvolve the GMI data to DPR resolution. Since unconstrained deconvolution would be highly sensitive to noise in the radiometer observations, the DPR-resolution brightness temperature ensembles are used to supply a high-resolution *a priori* constraint on the deconvolved brightness temperatures.

Estimates of GMI brightness temperatures at the DPR resolution are obtained using a variational approach. In this approach, a functional, $J$, of the estimated field of DPR-resolution brightness temperatures, $\mathbf{TB_{DPR}}$, is minimized, where

$$\begin{aligned} J\left(\mathbf{TB_{DPR}}\right) \equiv & \frac{1}{2}\left(\mathbf{TB_{obs}} - \mathbf{A}*\mathbf{TB_{DPR}}\right)^T \mathbf{W_{TB}^{-1}} \left(\mathbf{TB_{obs}} - \mathbf{A}*\mathbf{TB_{DPR}}\right) \\ & + \left(\mathbf{TB_{DPR}} - \left\langle \mathbf{TB_{DPRens}} \right\rangle\right)^T \mathbf{W}_{\mathbf{TB_{DPRens}}}^{-1} \left(\mathbf{TB_{DPR}} - \left\langle \mathbf{TB_{DPRens}} \right\rangle\right). \end{aligned} \tag{4}$$

Here, $\mathbf{TB_{obs}}$ is a vector of observed, GMI-resolution brightness temperatures, $\mathbf{A}$ is a matrix representing the GMI antenna patterns, $\mathbf{W_{TB}}$ is a matrix of observed brightness temperature error covariances (noise variances), $\langle\mathbf{TB_{DPRens}}\rangle$ is a vector of the ensemble-mean brightness temperatures derived from the Radar Module solutions, and $\mathbf{W_{TB\text{-}DPRens}}$ is a matrix of ensemble covariances, also derived from the Radar Module solutions. The first term of the functional represents the error of the DPR-resolution estimates relative to the observed brightness temperatures, and the second term represents the error of the estimates relative to the initial guess values derived from the Radar Module solutions. The functional $J$ is minimized by iteratively adjusting the field of $\mathbf{TB_{DPR}}$, using a quasi-Newton method. The success of the brightness temperature deconvolution depends upon the proper specification of the brightness temperature ensemble means $\langle\mathbf{TB_{DPRens}}\rangle$ and covariances $\mathbf{W_{TB\text{-}DPRens}}$, which in turn are dependent upon assumptions regarding the *a priori* distributions of water vapor, cloud water, precipitation particle-size parameters, and surface emissivities (or 10-meter wind speeds). In particular, the degree to which these parameters covary spatially, at the scale of GMI footprints, will lead to spatial covariances of $\mathbf{TB_{DPRens}}$ that will help to constrain the optimization of $\mathbf{TB_{DPR}}$.

Once the DPR-resolution brightness temperatures at the GMI channel frequencies and polarizations are estimated, they are used to perform a second ensemble Kalman filtering of the Radar Module profile ensembles to obtain final ensembles of water vapor, cloud water and $N_w/D_o/\mu$ profiles, and associated surface emissivities (or 10-meter wind speeds over water surfaces) at each DPR footprint location. The means of the final ensembles represent the best estimates of the parameters, and the standard deviations of the ensembles relative to the means represent uncertainties of the best estimates.

The following sections describe the current configuration of the primary modules of the Combined Radar-Radiometer Algorithm, including input and output parameters. Also described are Algorithm-supporting modules, datasets, and tables.

*Radar Module*

The basic function of the Radar Module is to ingest a granule (one orbit) of Level-2 calibrated DPR reflectivities and produce ensembles of DPR-consistent water vapor, cloud water, $\mu$, and precipitation $N_w/D_o$ profiles corresponding to each DPR footprint location. The inputs required are the calibrated $Z_{Ku}$ and $Z_{Ka}$ profiles at each DPR footprint location within the orbit. In addition, the Radar Module ingests total path-integrated attenuation estimates at Ku and Ka band and their uncertainties at each DPR footprint location from the SRT Module. The SRT Module is being developed by the GPM Radar Algorithm Team as one member of a suite of modules that support the Radar Algorithm.

In addition to radar reflectivities and path-integrated attenuation estimates, the Radar Module ingests estimates of the pressure, temperature, vapor density, and precipitation profile characteristics from the Profile Characterization Module. The current plan for the Profile Characterization Module is that it will deliver output from three algorithms provided by the Radar Algorithm Team: the Preparation Module determines if precipitation is detected in a given DPR reflectivity profile; the Vertical Profile Model provides profiles of pressure, temperature, and vapor density, interpolated to the DPR footprint locations and gate levels, based upon analysis data (or re-analysis climatology, for near real-time applications), and the Classification Module determines whether of not a bright-band of radar reflectivity is detected, the altitude of the bright-band, if it exists, and the classification of the DPR footprint as convective, stratiform, or indeterminate. The current analysis utilized by the Vertical Profile Module is the Japanese Meteorological Agency's operational analysis, and the re-analysis climatology is the Japanese 25-year Re-analysis.

The Radar Module also draws upon tabulated single-scattering parameters that have been pre-computed for the purpose of algorithm computational efficiency. The scattering parameters are calculated at the Ku and Ka bands, as well as the frequencies of the GMI, including the double side-band frequencies at 183.3 ± 7 and 183.3 ± 3 GHz. Tables of gaseous absorption coefficients are currently calculated as functions of pressure, temperature, and vapor density using the Millimeter-wave Propagation Model 1993 (see Liebe, 1989; Liebe et al. 1992). Tables of cloud water absorption coefficients are currently calculated as functions of temperature and equivalent liquid water content using Rayleigh theory. Because precipitation of all phases produces scattering as well as absorption/emission of microwaves, and since the particle size distribution as well as the water content of precipitation determines its bulk scattering and absorption/emission characteristics, separate databases are used to tabulate the single-scattering properties of precipitation. To limit the number of entries in these tables, only values of reflectivity, extinction coefficient, scattering coefficient, and asymmetry parameter, normalized by $N_w$, are tabulated. The table

entries are thus only functions of $D_o$ and $\mu$, and they provide an easy lookup for a given estimated $N_w$ and reflectivity.

As described in the *Overview*, above, the output of the Radar Module are ensembles of water vapor, cloud water, and $N_w/D_o/\mu$ profiles at each DPR footprint location.

*Surface Module*

The basic function of the Surface Module is to assign surface emissivities/reflectivities to each DPR-derived ensemble profile member, given the location, surface skin temperature, and 10-meter wind speed (if over a water surface) corresponding to the DPR footprint location. The surface skin temperature and 10-meter wind speed are currently derived from an analysis (or a re-analysis climatology for near real-time applications) in the Profile Characterization Module and interpolated to the DPR footprint location; see Radar Module description.

If the DPR footprint is over a water surface, a geometric optics/foam model is used to directly calculate the emissivities/reflectivities of the water surface, given the surface skin temperature, salinity (from climatology), 10-meter wind speed, and incidence angle. The culmination of research to date (see Wilheit 1979; English and Hewison 1998; Deblonde and English 2000; Ellison et al. 2003; Liu and Weng 2003; Boukabara and Weng 2008) has resulted in a fast emissivity model (FASTEM) that is now in its fourth generation; Weng (personal commun.). The current plan is to utilize this model to compute the surface emissivities/reflectivities of water surfaces at all GMI channel frequencies and polarizations. To obtain an *a priori* ensemble of emissivities/ reflectivities, Gaussian-distributed random perturbations of the analyzed skin temperature, salinity, and 10-meter wind speed are assumed to simulate uncertainties in the emissivity model input.

If the DPR footprint is over a land surface, a surface emissivity database is scanned to find an appropriate emissivity mean and standard deviation for that location. Here, it is assumed reflectivities can be derived from $r = 1 - e$, based upon Kirchhoff's law. The current plan is to re-sample land surface emissivities from emissivity climatologies developed by GPM investigators. For example, a 16-year, quarter-degree resolution dataset of emissivities based upon cloud-cleared SSM/I observations has been developed; see Prigent et al. (2006). This climatology was used to create a monthly, quarter-degree climatology of mean emissivities and their interchannel covariances that can be interpolated to the GMI frequencies and viewing angle using the Tool to Estimate Land Surface Emissivities in the Microwave (TELSEM) software; see Aires et al. (2010). An alternative monthly land emissivity/covariance database constructed from 11 years of rain-cleared TRMM observations has been developed by Masunaga and Furuzawa (personal commun.). Presently, both emissivity databases are being intercompared by the GPM Land Surface Working Group. Since emissivity interchannel covariance information is available for these emissivity databases, random perturbations of emissivities/reflectivities having the observed covariance characteristics can be

generated to create ensembles. The grouping of emissivities into self-similar classes, and the utilization of an EOF representation of the emissivities in each class, will reduce the memory required to hold the emissivity database.

Both land surface microwave emission and precipitation emission/scattering in the overlying atmosphere are variable in space and time, and they are often difficult to separate in radiometric measurements. Contamination by precipitation signals, therefore, can be a large source of uncertainty in land surface emissivity estimates, and this has been a challenge to existing algorithms. The GPM core observatory, unlike other satellite platforms carrying only radiometers, has the advantage that the presence or absence of DPR radar echo within a collocated GMI field of view will provide an accurate rain screening to filter out precipitating scenes on an instantaneous basis. Therefore, it is anticipated that a future modification of the Surface Module would be to estimate emissivities in precipitation-free areas of a given orbit and interpolate those emissivities into precipitating areas. This kind of dynamic updating would produce more contemporaneous estimates of emissivities/reflectivities than those derived from a static climatology. Dynamic updating of emissivities can also be accomplished using meteorological analysis data coupled to a land surface model, which together can be used to provide input to a physically-based emissivity model. These possibilities for dynamic emissivity updating are currently under investigation by the GPM Land Surface Working Group.

The ensembles of emissivities/reflectivities over water or land surfaces are assigned at random to the ensembles of DPR-derived profiles at each DPR footprint location, and the profiles and assigned emissivities/reflectivities are output to the Radiative Transfer Module.

*Radiative Transfer Module*

The basic function of the Radiative Transfer Module is to compute upwelling brightness temperatures at the GMI channel frequencies/polarizations and viewing angle, given the input ensembles of DPR-derived profiles from the Radar Module and emissivities/reflectivities assigned to those profiles in the Surface Module. The single-scattering parameters associated with the ensembles of DPR-derived profiles of water vapor, cloud water, and precipitation $N_w/D_o/\mu$ profiles are calculated using the gaseous/cloud absorption and precipitation scattering tables, described in the Radar Module section, above. The given pressures, temperatures, vapor densities, and cloud liquid-equivalent water contents of each profile are used to derive appropriate absorption coefficients at the GMI channel frequencies. The $N_w$ values of each profile can be used to rescale the normalized extinction, scattering, and asymmetry parameters, filed as functions of $D_o$ and $\mu$, in the tables. The gaseous, cloud water, and precipitation single-scattering parameters, as well as the assigned surface emissivities/reflectivities, are then passed to a forward radiative transfer model to compute upwelling brightness temperatures. Currently, these calculations are performed using Eddington's Second Approximation for radiative transfer (Kummerow 1993; Olson et al. 2001), which is computationally efficient and accurate for the range of GMI channel frequencies. The output is an ensemble of

brightness temperatures at the GMI channel frequencies/polarizations and viewing angle, at each DPR footprint location and at the horizontal resolution of the DPR.

*Inversion Module*

The function of the Inversion Module is to deconvolve the relatively low-resolution GMI brightness temperatures to approximately DPR resolution, using the ensembles of DPR-derived brightness temperatures as constraints, and to then perform an ensemble Kalman filtering of the DPR-derived profile ensembles from the radar model. Inputs are the Level-1 calibrated GMI brightness temperatures over one granule (one orbit, including two 50-scan overlap fields) and the fields of DPR-derived brightness temperature ensembles over the DPR swath, drawn from the Radiative Transfer Module. The deconvolution procedure yields estimates of the GMI brightness temperatures at DPR resolution (5 km) at each DPR footprint location. The DPR-resolution brightness temperatures are then used to perform an ensemble Kalman filter update of the DPR-derived ensembles of water vapor, cloud water, and precipitation $N_w/D_o/\mu$ profiles from the Radar Module and associated surface emissivities (or 10-meter wind speed over water surfaces) from the Surface Module. The final output are the means (best estimates) and standard deviations (uncertainties) of the filtered ensemble parameters.

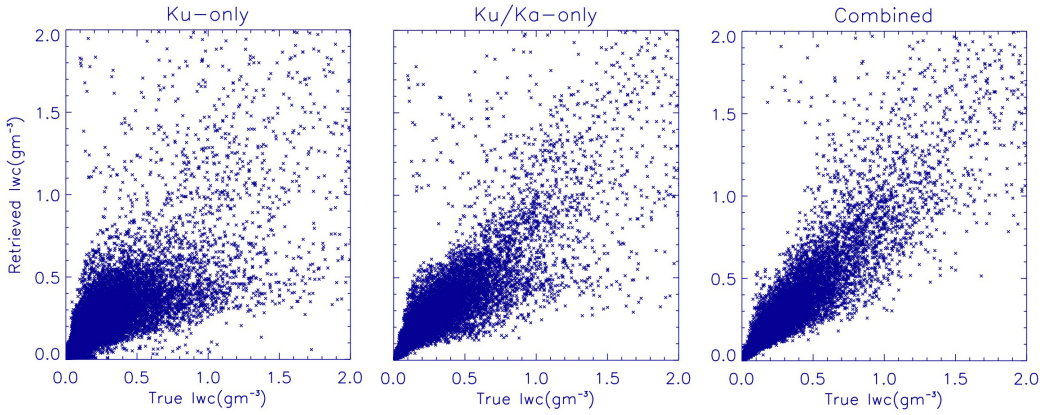


*Fig. 3. Estimated vs. true water contents derived from applications of the Combined Radar-Radiometer Algorithm to synthesized airborne radar-radiometer observations. Separate scatterplots illustrate the impact of only Ku-band radar data (left), only Ku- and Ka-band radar data (middle), and combined Ku/Ka band radar and 10-85 GHz passive microwave observations (right) on retrieved water contents.*

Shown in Fig. 3 are scatterplots from prototype Combined Algorithm applications to synthesized airborne radar-radiometer observations of tropical precipitation. As more information is introduced into the procedure, more specific estimates of precipitation liquid water contents are achieved, and the scatter of estimates is reduced relative to the synthesized "true" water contents. This test illustrates the mechanics of the algorithm in an application to collocated, high-resolution, nadir-

view observations; DPR-GMI applications will require deconvolution of GMI brightness temperatures as described in the *Overview* of this section.

## 4. Output Precipitation Products

The current planning is for two output precipitation profile products. The primary product draws upon information from DPR Ku- and Ka-band reflectivities and total path-integrated attenuation estimates, as well as GMI brightness temperatures, over the DPR Ku-Ka band overlap swath. This product will be the main tool for cross-calibrating the GPM radiometer precipitation estimates through the creation of *a priori* databases. A second product will draw upon information from DPR Ku-band reflectivities and total path-integrated attenuation estimates, as well as GMI brightness temperatures, over the DPR Ku-band swath. The algorithm architecture is the same for creating either product.

## 5. Summary of Input/Output Parameters

The listing of input and output parameters, below, is tentative. Some of the input parameters will be provided by output of modules developed by the GPM Radar Algorithm Team, and their modules are under construction. Still, the listing is fairly representative of the parameters that are needed.

*Input Parameters*

This listing includes only those parameters that will be ingested from modules that are external to the Combined Radar-Radiometer Algorithm code. The given array sizes correspond to 49 rays of Ku-band data and 25 rays of matched-beam Ka-band data, with 200 range bins per ray, and 24 rays of Ka-band high-sensitivity mode data, with 100 range bins per ray, per DPR "scan". Also, it is assumed that there are 221 footprints of both low-frequency (≤ 89 GHz) and high-frequency (>89 GHz) data per GMI “scan”.

**latitude_PRE**
latitudes of DPR footprints ((49+49) x 4 bytes); from the Radar Algorithm Preparation Module.

**longitude_PRE**
longitudes of DPR footprints ((49+49) x 4 bytes); from the Radar Algorithm Preparation Module.

**year_of_scan_PRE**
year of the DPR scan (2 x 2 bytes); from the Radar Algorithm Preparation Module..

**month_of_scan_PRE**
month of the DPR scan (2 x 1 bytes); from the Radar Algorithm Preparation Module.

**day_of_scan_PRE**
day of the DPR scan (2 x 1 bytes); from the Radar Algorithm Preparation Module.

**hour_of_scan_PRE**
hour of the DPR scan (2 x 1 bytes); from the Radar Algorithm Preparation Module.

**minute_of_scan_PRE**
minute of the DPR scan (2 x 1 bytes); from the Radar Algorithm Preparation Module.

**second_of_scan_PRE**
second of the DPR scan (2 x 1 bytes); from the Radar Algorithm Preparation Module.

**millisecond_of_scan_PRE**
millisecond of the DPR scan (2 x 1 bytes); from the Radar Algorithm Preparation Module.

**surface_elevation_PRE**
altitudes above the Earth ellipsoid of the surface gates in DPR rays ((49+49) x 4 bytes); from the Radar Algorithm Preparation Module.

**surface_type_PRE**
water/land/coast and surface types at DPR footrpint locations ((49+49) x 4 bytes); from the Radar Algorithm Preparation Module. Note that this information is used to interpret surface reference technique output.

**local_zenith_angle_PRE**
local incidence angles of DPR rays relative to local zenith on the Earth ellipsoid ((49+49) x 4 bytes); from the Radar Algorithm Preparation Module.

**precipitation_flag_PRE**
flags indicating detection of precipation or no precipitation in DPR rays ((49+49) x 4 bytes); from the Radar Algorithm Preparation Module.

**surface_range_bin_PRE**
surface range bins in DPR rays ((49+49) x 4 bytes); from the Radar Algorithm Preparation Module.

**lowest_clutterfree_bin_PRE**
range bins of the lowest clutter-free bins of DPR rays ((49+49) x 4 bytes); from the Radar Algorithm Preparation Module.

**sigma_zero_PRE**
measured surface normalized backscattering radar cross-sections of DPR ((49+49) x 4 bytes); from the Radar Algorithm Preparation Module.

**measured_reflectivity_factor_PRE**
measured calibrated reflectivities of the DPR ((49+25) x 200 x 4 bytes + 24 x 100 x 4 bytes); from the Radar Algorithm Preparation Module.

**midpoint_range_bin_altitude_PRE**
computed altitudes of the midpoints of DPR range bins relative to the ellipsoid ((49+25) x 200 x 4 bytes + 24 x 100 x 4 bytes); from the Radar Algorithm Preparation Module.

**air_temperature_VER**
air temperatures interpolated to DPR range bins ((49 + 25) x 200 x 4 bytes + 24 x 100 x 4 bytes); from JMA analysis using the Radar Algorithm Vertical Profile Module, or JRA-25 for near real-time processing.

**zero_degree_bin_VER**
range bins containing the zero-degree levels ((49 + 49) x 4 bytes); based upon interpolated JMA analysis using the Radar Algorithm Vertical Profile Module, or JRA-25 for near real-time processing.

**air_pressure_VER**
air pressures interpolated to DPR range bins ((49+25) x 200 x 4 bytes + 24 x 100 x 4 bytes); from JMA analysis using the Radar Algorithm Vertical Profile Module, or JRA-25 for near real-time processing.

**vapor_density_VER**
water vapor densities interpolated to DPR range bins ((49+25) x 200 x 4 bytes + 24 x 100 x 4 bytes); from JMA analysis using the Radar Algorithm Vertical Profile Module, or JRA-25 for near real-time processing.

**cloud_liquid_water_content_VER**
cloud liquid water contents interpolated to DPR range bins ((49+25) x 200 x 4 bytes + 24 x 100 x 4 bytes); from JMA analysis using the Radar Algorithm Vertical Profile Module, or JRA-25 for near real-time processing.

**cloud_ice_water_content_VER**
cloud ice liquid-equivalent water contents interpolated to DPR range bins ((49+25) x 200 x 4 bytes + 24 x 100 x 4 bytes); from JMA analysis using the Radar Algorithm Vertical Profile Module, or JRA-25 for near real-time processing.

**zero_degree_altitude_VER**
altitudes of the zero-degree levels along DPR range bins ((49 + 49) x 4 bytes); based upon interpolated JMA analysis using the Radar Algorithm Vertical Profile Module, or JRA-25 for near real-time processing.

**surface_air_pressure_VER**
surface air pressures interpolated to the DPR footprint locations ((49+49) x 4 bytes); from JMA analysis using the Radar Algorithm Vertical Profile Module, or JRA-25 for near real-time processing.

**ground_temperature_VER**
surface skin temperatures interpolated to DPR footprint locations ((49+49) x 4 bytes); from JMA analysis using the Radar Algorithm Vertical Profile Module, or JRA-25 for near real-time processing.

**ten_meter_wind_speed_VER**
10-meter wind speeds interpolated to DPR footprint locations ((49+49) x 4 bytes); from JMA analysis using the Radar Algorithm Vertical Profile Module, or JRA-25 for near real-time processing.

**bright_band_detection_flag_CSF**
flags indicating the detection of a bright-band in DPR rays ((49+49) x 4 bytes); from the Radar Algorithm Classification Module.

**bright_band_peak_bin_CSF**
range bins of the bright-band maximum reflectivities, if detected, in DPR rays ((49+49) x 4 bytes); from the Radar Algorithm Classification Module.

**bright_band_peak_altitude_CSF**
altitudes of the bright-band maximum reflectivities, if detected, in DPR rays ((49+49) x 4 bytes); from the Radar Algorithm Classification Module.

**bright_band_detection_quality_flag_CSF**
quality flags for bright band detection in DPR rays ((49+49) x 4 bytes); from the Radar Algorithm Classification Module.

**precipitation_type_CSF**
classifications of precipitation type in DPR rays ((49 + 49) x 4 bytes); from the Radar Algorithm Classification Module.

**precipitation_type_quality_flag_CSF**
quality of classifications of precipitation type in DPR rays ((49 + 49) x 4 bytes); from the Radar Algorithm Classification Module.

**pia_SRT**
total 2-way path-integrated attenuations to the surface based upon surface reference technique methods for Ku-only, Ka-only, Ka high-sensitivity mode, and Ku+Ka (49 x 5 x 4 bytes + 25 x 5 x 4 bytes + 24 x 5 x 4 bytes + 25 x 2 x 4 bytes); from the Radar Algorithm Surface Reference Technique Module.

**pia_reliability_factor_SRT**
reliability factors of total 2-way path-integrated attenuation estimates based upon surface reference technique methods for Ku-only, Ka-only, Ka high-sensitivity mode, and Ku+Ka (49 x 5 x 4 bytes + 25 x 5 x 4 bytes + 24 x 5 x 4 bytes + 25 x 2 x 4); from the Radar Algorithm Surface Reference Technique Module.

**pia_weight_SRT**
weights of individual 2-way total path-integrated attenuation estimates to form effective estimates for Ku-only, Ka-only, and Ka high-sensitivity mode (49 x 5 x 4 bytes + 25 x 5 x 4 bytes + 24 x 5 x 4 bytes); from the Radar Algorithm Surface Reference Technique Module.

**pia_effective_SRT**
total 2-way path-integrated attenuations to the surface based upon weighted averages of surface reference technique methods for Ku-only, Ka-only, and Ka high-sensitivity mode (49 x 4 bytes + 25 x 4 bytes + 24 x 4 bytes); from the Radar Algorithm Surface Reference Technique Module.

**pia_effective_reliability_factor_SRT**
reliability factors of composite total 2-way path-integrated attenuation estimates based upon surface reference technique methods for Ku-only, Ka-only, and Ka high-sensitivity mode (49 x 4 bytes + 25 x 4 bytes + 24 x 4 bytes); from the Radar Algorithm Surface Reference Technique Module.

**pia_effective_error_variance_SRT**
error variances of the effective total 2-way path-integrated attenuation estimates based upon weighted averages of surface reference technique methods for Ku-only, Ka-only, Ka high-sensitivity mode, and Ku+Ka (49 x 4 bytes + 25 x 4 bytes + 24 x 4 bytes + 25 x 2 x 4 bytes); from the Radar Algorithm Surface Reference Technique Module.

**latitude_GMI**
latitudes of the GMI footprints ((221+221) x 2 bytes); from the Level-1 GMI processing. Note that the GMI channels ≤ 89 GHz and those > 89 GHz have different scan patterns. Also, the number of footprints per GMI scan is still under discussion; assumed to be 221, here.

**longitude_GMI**
longitudes of the GMI footprints ((221+221) x 2 bytes); from the Level-1 GMI processing. Note that the GMI channels ≤ 89 GHz and those > 89 GHz have different scan patterns. Also, the number of footprints per GMI scan is still under discussion; assumed to be 221, here.

**time_of_scan_GMI**
time of the beginning of the GMI scan (7 bytes); from the Level-1 GMI processing.

**brightness_temperature_GMI**
calibrated GMI brightness temperatures in 13 channels (221 x 9 x 2 bytes + 221 x 4 x 2 bytes); from the Level-1 GMI processing. Note that the number of footprints per GMI scan is still under discussion; assumed to be 221, here.

*Output Parameters (Standard Processing)*

The array sizes given correspond to a single scan of the DPR. Note standard output products are sampled at 250 m vertical resolution.

**latitude_CMB**
latitudes of DPR Ku-band footprints (49 x 4 bytes); from the Radar Algorithm Preparation Module.

**longitude_CMB**
longitudes of DPR Ku-band footprints (49 x 4 bytes); from the Radar Algorithm Preparation Module.

**year_of_scan_CMB**
year of the DPR Ku-band scan (1 x 2 bytes); from the Radar Algorithm Preparation Module..

**month_of_scan_CMB**
month of the DPR Ku-band scan (1 x 1 bytes); from the Radar Algorithm Preparation Module.

**day_of_scan_CMB**
day of the DPR Ku-band scan (1 x 1 bytes); from the Radar Algorithm Preparation Module.

**hour_of_scan_CMB**
hour of the DPR Ku-band scan (1 x 1 bytes); from the Radar Algorithm Preparation Module.

**minute_of _scan_CMB**
minute of the DPR Ku-band scan (1 x 1 bytes); from the Radar Algorithm Preparation Module.

**second_of_scan_CMB**
second of the DPR Ku-band scan (1 x 1 bytes); from the Radar Algorithm Preparation Module.

**millisecond_of_scan_CMB**
millisecond of the DPR Ku-band scan (1 x 1 bytes); from the Radar Algorithm Preparation Module.

**surface_elevation_CMB**
altitudes above the Earth ellipsoid of the surface gates in DPR Ku-band rays (49 x 4 bytes); from the Radar Algorithm Preparation Module.

**surface_type_CMB**
water/land/coast and surface types at DPR Ku-band footrpint locations (49 x 4 bytes); from the Radar Algorithm Preparation Module. Note that this information is used to interpret surface reference technique output.

**local_zenith_angle_CMB**

local incidence angles of DPR Ku-band rays relative to local zenith on the Earth ellipsoid (49 x 4 bytes); from the Radar Algorithm Preparation Module.

**precipitation_flag_CMB**
flags indicating detection of precipation or no precipitation in DPR Ku-band rays (49 x 4 bytes); from the Radar Algorithm Preparation Module.

**surface_range_bin_CMB**
surface range bins in DPR Ku-band rays (49 x 4 bytes); from the Radar Algorithm Preparation Module.

**lowest_clutterfree_bin_CMB**
range bins of the lowest clutter-free bins of DPR Ku-band rays (49 x 4 bytes); from the Radar Algorithm Preparation Module.

**sigma_zero_CMB**
measured surface normalized backscattering radar cross-sections of DPR at Ku- and Ka-bands ((49+25) x 4 bytes); from the Radar Algorithm Preparation Module.

**measured_reflectivity_factor_CMB**
measured calibrated reflectivities of the DPR Ku- and Ka-band rays at 250 m sampling resolution ((49+25) x 100 x 2 bytes); from the Radar Algorithm Preparation Module.

**midpoint_range_bin_altitudes_CMB**
computed altitudes of the midpoints of DPR Ku-band range bins at 250 m sampling resolution relative to the ellipsoid (49 x 100 x 2 bytes); from the Radar Algorithm Preparation Module.

**air_temperature_CMB**
air temperatures interpolated to DPR Ku-band range bins at 250 m sampling resolution (49 x 100 x 2 bytes); from JMA analysis using the Radar Algorithm Vertical Profile Module.

**zero_degree_bin_CMB**
Ku-band range bins containing the zero-degree levels (49 x 4 bytes); based upon interpolated JMA analysis using the Radar Algorithm Vertical Profile Module.

**air_pressure_CMB**
air pressures interpolated to DPR Ku-band range bins at 250 m resolution (49 x 100 x 2 bytes); from JMA analysis using the Radar Algorithm Vertical Profile Module.

**vapor_density_init_CMB**
water vapor densities interpolated to DPR Ku-band range bins at 250 m resolution (49 x 100 x 2 bytes); from JMA analysis using the Radar Algorithm Vertical Profile Module.

**cloud_liquid_water_content_init_CMB**
cloud liquid water contents interpolated to DPR Ku-band range bins at 250 m sampling resolution (49 x 100 x 2 bytes); from JMA analysis using the Radar Algorithm Vertical Profile Module.

**cloud_ice_water_content_init_CMB**
cloud ice liquid-equivalent water contents interpolated to DPR Ku-band range bins at 250 m sampling resolution (49 x 100 x 2 bytes); from JMA analysis using the Radar Algorithm Vertical Profile Module.

**zero_degree_altitude_init_CMB**
altitudes of the zero-degree levels along DPR Ku-band range bins (49 x 4 bytes); based upon interpolated JMA analysis using the Radar Algorithm Vertical Profile Module.

**surface_air_pressure_CMB**
surface air pressures interpolated to the DPR Ku-band footprint locations (49 x 4 bytes); from JMA analysis using the Radar Algorithm Vertical Profile Module.

**ground_temperature_CMB**
surface skin temperatures interpolated to DPR Ku-band footprint locations (49 x 4 bytes); from JMA analysis using the Radar Algorithm Vertical Profile Module.

**ten_meter_wind_speed_init_CMB**
10-meter wind speeds interpolated to DPR Ku-band footprint locations (49 x 4 bytes); from JMA analysis using the Radar Algorithm Vertical Profile Module.

**bright_band_detection_flag_CMB**
flags indicating the detection of a bright-band in DPR Ku- and Ka-band rays ((49+25) x 4 bytes); from the Radar Algorithm Classification Module.

**bright_band_peak_bin_CMB**
range bins of the bright-band maximum reflectivities, if detected, in DPR Ku- and Ka-band rays ((49+25) x 4 bytes); from the Radar Algorithm Classification Module.

**bright_band_peak_altitude_CMB**
altitudes of the bright-band maximum reflectivities, if detected, in DPR Ku- and Ka-band rays ((49+25) x 4 bytes); from the Radar Algorithm Classification Module.

**bright_band_detection_quality_flag_CMB**
quality flags for bright band detection in DPR Ku- and Ka-band rays ((49+25) x 4 bytes); from the Radar Algorithm Classification Module.

**precipitation_type_CMB**
classifications of precipitation type in DPR Ku-band rays (49 x 4 bytes); from the Radar Algorithm Classification Module.

**precipitation_type_quality_flag_CMB**
quality of classifications of precipitation type in DPR Ku-band rays (49 x 4 bytes); from the Radar Algorithm Classification Module.

**pia_CMB**
total 2-way path-integrated attenuations to the surface based upon surface reference technique methods for Ku-only, Ka-only, and Ku+Ka (49 x 5 x 4 bytes + 25 x 5 x 4 bytes + 25 x 2 x 4 bytes); from the Radar Algorithm Surface Reference Technique Module.

**pia_reliability_factor_CMB**
reliability factors of total 2-way path-integrated attenuation estimates based upon surface reference technique methods for Ku-only, Ka-only, and Ku+Ka (49 x 5 x 4 bytes + 25 x 5 x 4 bytes + 25 x 2 x 4 bytes); from the Radar Algorithm Surface Reference Technique Module.

**pia_weight_CMB**
weights of individual 2-way total path-integrated attenuation estimates to form effective estimates for Ku-only and Ka-only (49 x 5 x 4 bytes + 25 x 5 x 4 bytes); from the Radar Algorithm Surface Reference Technique Module.

**pia_effective_CMB**
total 2-way path-integrated attenuations to the surface based upon weighted averages of surface reference technique methods for Ku-only and Ka-only (49 x 4 bytes + 25 x 4 bytes); from the Radar Algorithm Surface Reference Technique Module.

**pia_effective_reliability_factor_CMB**
reliability factors of composite total 2-way path-integrated attenuation estimates based upon surface reference technique methods for Ku-only and Ka-only (49 x 4 bytes + 25 x 4 bytes); from the Radar Algorithm Surface Reference Technique Module.

**pia_effective_error_variance_CMB**
error variances of the effective total 2-way path-integrated attenuation estimates based upon weighted averages of surface reference technique methods for Ku-only, Ka-only, and Ku+Ka (49 x 4 bytes + 25 x 4 bytes + 25 x 2 x 4 bytes); from the Radar Algorithm Surface Reference Technique Module.

**vapor_density_out_CMB**
vapor densities along the DPR rays at 250 m sampling resolution ((49+25) x 100 x 2 bytes); from the Combined Algorithm.

**cloud_liquid_water_content_out_CMB**
cloud liquid water contents along the DPR rays at 250 m sampling resolution ((49+25) x 100 x 2 bytes); from the Combined Algorithm.

**cloud_ice_water_content_out_CMB**
cloud ice liquid-equivalent water contents along the DPR rays at 250 m sampling resolution ((49+25) x 100 x 2 bytes); from the Combined Algorithm.

**rain_psd_parameter_out_CMB**
liquid precipitation drop-size distribution parameters ($\log(N_w)$, $D_o$, $\mu$) along the DPR rays at 250 m sampling resolution ((49+25) x 100 x 3 x 2 bytes); from the Combined Algorithm.

**rain_psd_parameter_sigma_out_CMB**
liquid precipitation drop-size distribution parameter ($\log(N_w)$, $D_o$, $\mu$) uncertainties along the DPR rays at 250 m sampling resolution ((49+25) x 100 x 3 x 2 bytes); from the Combined Algorithm.

**ice_psd_parameter_out_CMB**
ice-phase precipitation liquid-equivalent drop-size distribution parameters ($\log(N_w)$, $D_o$, $\mu$) along the DPR rays at 250 m sampling resolution ((49+25) x 100 x 3 x 2 bytes); from the Combined Algorithm.

**ice_psd_parameter_sigma_out_CMB**
ice-phase precipitation liquid-equivalent drop-size distribution parameter ($\log(N_w)$, $D_o$, $\mu$) uncertainties along the DPR rays at 250 m vertical resolution ((49+25) x 100 x 3 x 2 bytes); from the Combined Algorithm.

**ice_density_out_CMB**
density of ice-phase precipitation expressed as a power law ($\alpha$, $\beta$, of $\rho_{ice} = \alpha D^{\beta}$, where D is particle melted diameter) along the DPR rays at 250 m sampling resolution ((49+25) x 100 x 2 x 2 bytes); from the Combined Algorithm.

**ice_melt_fraction_out_CMB**
fractions of melting ice particle liquid-equivalent water content in the form of liquid water along the DPR rays at 250 m sampling resolution ((49+25) x 100 x 2 bytes); from the Combined Algorithm.

**surface_rainfall_rate_out_CMB**
surface liquid precipitation rates ((49+25) x 2 bytes); from the Combined Algorithm.

**surface_rainfall_rate_sigma_out_CMB**
surface liquid precipitation rate uncertainties ((49+25) x 2 bytes); from the Combined Algorithm.

**surface_precip_ice rate_out_CMB**
surface ice-phase precipitation rates ((49+25) x 2 bytes); from the Combined Algorithm.

**surface_precip_ice_rate_sigma_out_CMB**
surface ice-phase precipitation rate uncertainties ((49+25) x 2 bytes); from the Combined Algorithm.

**pia_out_CMB**
total path-integrated attenuations at the DPR footprint locations (49 x 4 bytes + 25 x 2 x 4 bytes); from the Combined Algorithm.

**corrected_reflectivity_factor_out_CMB**
attenuation-corrected radar reflectivity factors along the DPR rays at 250 m sampling resolution (49 x 100 x 2 bytes + 25 x 100 x 2 x 2 bytes); from the Combined Algorithm.

**ten_meter_wind_speed_out_CMB**
10-meter wind speeds ((49 +25) x 2 bytes); from the Combined Algorithm.

**surface_emissivity_out_CMB**
microwave surface emissivities at the GMI channel frequencies/polarizations, including separate emissivities for the double side-band channels at 183.3 ± 7 and 183.3 ± 3 GHz ((49 + 25) x 15 x 2 bytes); from the Combined Algorithm.

**simulated_brightness_temperature_out_CMB**
upwelling microwave surface brightness temperatures at the GMI channel frequencies/polarizations and viewing angle, but at DPR resolution, including separate brightness temperatures for the double side-band channels at 183.3 ± 7 and 183.3 ± 3 GHz ((49 + 25) x 15 x 2 bytes); from the Combined Algorithm.

*Output Parameters (Near Real-Time Processing)*

The array sizes given correspond to a single scan of the DPR.

**latitude_CMB**
latitudes of DPR Ku-band footprints (49 x 4 bytes); from the Radar Algorithm Preparation Module.

**longitude_CMB**
longitudes of DPR Ku-band footprints (49 x 4 bytes); from the Radar Algorithm Preparation Module.

**year_of_scan_CMB**
year of the DPR Ku-band scan (1 x 2 bytes); from the Radar Algorithm Preparation Module..

**month_of_scan_CMB**
month of the DPR Ku-band scan (1 x 1 bytes); from the Radar Algorithm Preparation Module.

**day_of_scan_CMB**
day of the DPR Ku-band scan (1 x 1 bytes); from the Radar Algorithm Preparation Module.

**hour_of_scan_CMB**
hour of the DPR Ku-band scan (1 x 1 bytes); from the Radar Algorithm Preparation Module.

**minute_of _scan_CMB**
minute of the DPR Ku-band scan (1 x 1 bytes); from the Radar Algorithm Preparation Module.

**second_of_scan_CMB**
second of the DPR Ku-band scan (1 x 1 bytes); from the Radar Algorithm Preparation Module.

**millisecond_of_scan_CMB**
millisecond of the DPR Ku-band scan (1 x 1 bytes); from the Radar Algorithm Preparation Module.

**surface_elevation_CMB**
altitudes above the Earth ellipsoid of the surface gates in DPR Ku-band rays (49 x 4 bytes); from the Radar Algorithm Preparation Module.

**surface_type_CMB**
water/land/coast and surface types at DPR Ku-band footrpint locations (49 x 4 bytes); from the Radar Algorithm Preparation Module. Note that this information is used to interpret surface reference technique output.

**precipitation_type_CMB**
classifications of precipitation type in DPR Ku-band rays (49 x 4 bytes); from the Radar Algorithm Classification Module.

**precipitation_type_quality_flag_CMB**
quality of classifications of precipitation type in DPR Ku-band rays (49 x 4 bytes); from the Radar Algorithm Classification Module.

**surface_rainfall_rate_out_CMB**
surface liquid precipitation rates ((49+25) x 2 bytes); from the Combined Algorithm.

**surface_rainfall_rate_sigma_out_CMB**
surface liquid precipitation rate uncertainties ((49+25) x 2 bytes); from the Combined Algorithm.

**surface_precip_ice rate_out_CMB**
surface ice-phase precipitation rates ((49+25) x 2 bytes); from the Combined Algorithm.

**surface_precip_ice_rate_sigma_out_CMB**
surface ice-phase precipitation rate uncertainties ((49+25) x 2 bytes); from the Combined Algorithm.

*Output Product Volumes*

The volume of the Combined Algorithm standard output product, based upon the output parameters listed above, is approximately 2.9 GB per orbit assuming 7900 DPR scans per orbit. Since precipitation only occurs over 5-10% of the earth's surface at any particular time, many of the precipitation parameters in the output

product will be either zero or a flagged as missing; therefore, the output product files are expected to compress by a factor of 10, at least.

To facilitate internet transfer of data, the Combined Algorithm near real-time product is much smaller; about 14 MB per orbit. This reduced product retains only the surface precipitation rates and their uncertainties.

## 6. Ancillary Datasets

In the current algorithm formulation, only the Analysis Data, below, must be ingested from an external source. The other tables and databases are static and will be read into memory upon the execution of the algorithm software.

*Analysis Data*

Analysis data will be required to produce initial estimates of environmental parameters such as surface skin temperature, 10-meter wind speed, and atmospheric profiles of pressure, temperature, vapor density, and cloud liquid and ice water contents. The current algorithm design will require space-time interpolation of these quantities from the Japanese Meteorological Agency's operational analysis during standard algorithm processing. These data will be interpolated using the Vertical Profile Module software provided by the GPM Radar Algorithm Team. For near real-time processing, the publically-available Japanese 25-year Re-analysis will be substituted for the JMA analysis data.

*Single-Scattering Tables*

Two types of tables will be produced by the GPM Radar Algorithm and Combined Algorithm Teams. The first table type will contain absorption coefficients for atmospheric gaseous constituents indexed by pressure, temperature, and humidity, and cloud water/ice absorption coefficients indexed by temperature and liquid-equivalent cloud water content. The second table type will contain normalized reflectivities, extinction coefficients, scattering coefficients, and asymmetry parameters. These parameters will be integrated over an assumed gamma distribution and normalized by the intercept, $N_w$, of that distribution; see (2). The integrated, normalized parameters will be indexed by $D_o$ and $\mu$, which determine the shape of the normalized gamma distribution. Separate tables will be created for liquid and ice-phase precipitation at different temperatures, and for mixed-phase precipitation, tables will be created for different displacements relative to the freezing level.

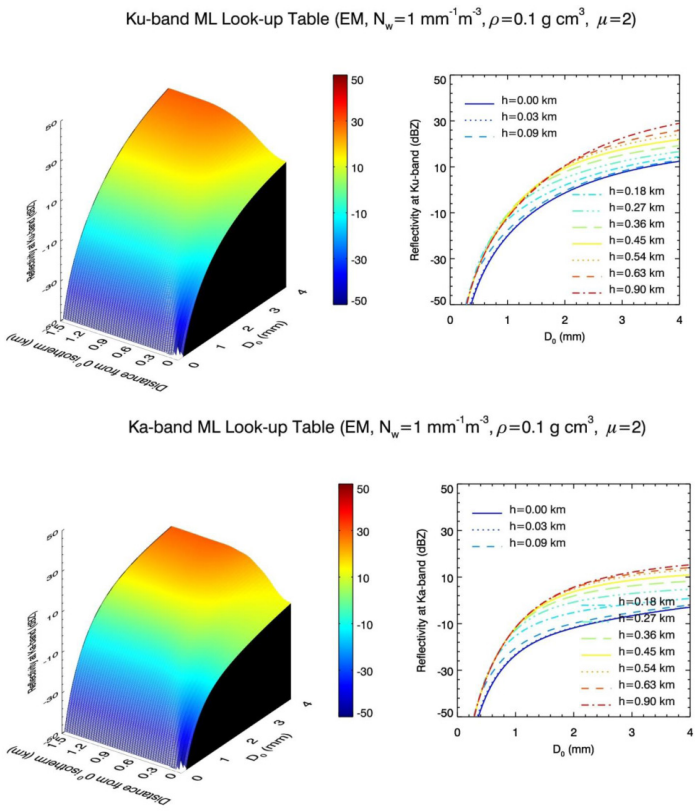


*Fig. 4. Graphical illustrations of Ku-band (top) and Ka-band (bottom) scattering tables entries for radar reflectivities within the melting layer. Color plots show the variation of reflectivity (given $N_w$) with both $D_o$ and distance below the 0°C level. Line plots show the same information for specific depths below the 0°C level.*

A graphical illustration of entries in the second table type is shown in Fig. 4 for Ku- and Ka-band reflectivities of melting snow particle distributions at various depths below the freezing level. The initial snow particles and partially-melted particles are assumed to be homogeneous, spherical ice-air or ice-air-liquid mixtures. Anticipated particle modeling improvements will include non-spherical melting snow, but the form of the tables will remain essentially unchanged, facilitating comparisons of different particle models on Combined Algorithm performance.

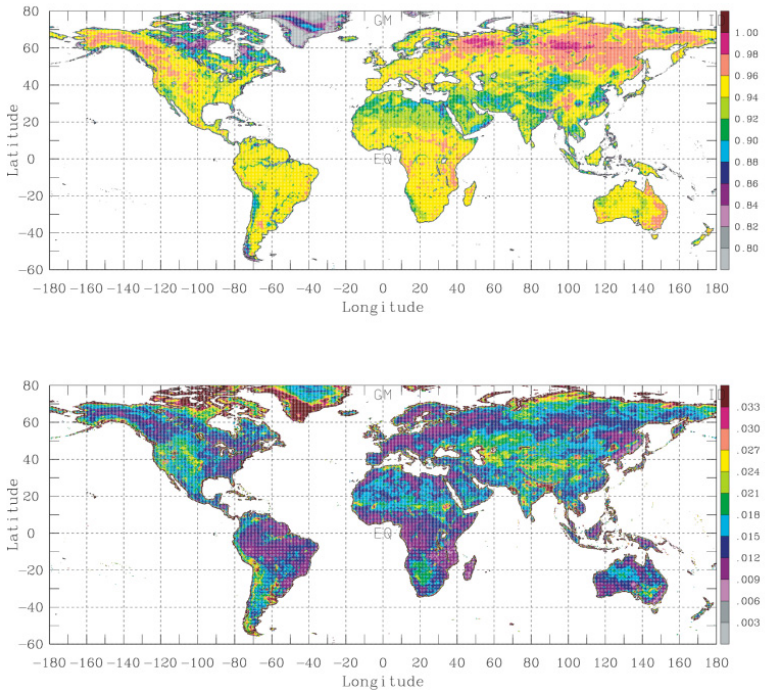


*Fig. 5. TELSEM mean emissivity estimates at 31.4 GHz (top), together with the corresponding emissivity standard deviations (bottom) from the TELSEM covariance matrices.*

*Surface Type Database*

This database will contain a gridded land/water classification and surface elevation over land. The database will have a horizontal sampling resolution of approximately 1 km, and several candidate databases are under consideration, including the SRTM30. Land cover parameters and elevation will be averaged to 5 km resolution to reflect the spatial resolution of measurements from the DPR.

*Surface Emissivity Database*

This database will contain latitude/longitude-indexed microwave surface emissivities and flux emissivities at the GMI channel frequencies/polarizations and viewing angle for classified surface types. The current plan is to develop this database in collaboration with the GPM Land Surface Working Group, starting with the TELSEM software/dataset of Aires et al. (2010). Shown in Fig. 5 are global distributions of TELSEM-derived mean emissivities and emissivity standard deviations drawn from the corresponding TELSEM covariance matrices.

## 7. Processing Requirements

The current configuration of the Combined Algorithm will require input from four modules of the GPM Radar Algorithm: the Preparation Module, the Vertical Profile

Module, the Classification Module, and the Surface Reference Technique Module. Output of these modules is expected from the main Radar Algorithm routine; however, the computational requirements of this routine could add significant latency to Combined Algorithm processing. Therefore, separate execution of the four Modules as a front-end to the Combined Algorithm should be considered for near real-time processing.

A primary input to the Vertical Profile Module in standard processing (non-near-real-time mode) will come from the JMA operational analysis (GANAL). Therefore, this input should be accommodated in PPS operations.

The current 1-D version of the algorithm (no brightness temperature deconvolution) requires 3 minutes on a single processor to process 3000 PR footprints. A typical orbit of DPR data will have 20,000 – 30,000 rain-affected footprints. This indicates roughly 30 minutes processing time per orbit using a single processor. Although some economies in the coding can reduce this processing time, they may result in degraded performance of the algorithm. The preferred alternative is to use multi-processing capability at PPS with the equivalent of ~10 CPU to reduce the overall processing time to 3 minutes/orbit, plus the time required to perform the brightness temperature deconvolution. Granules of DPR and GMI data will be subdivided into segments that will be processed in parallel. Parallel processing will be achieved using POSIX thread libraries.

## 8. References


Aires, F., C. Prigent, F. Bernardo, C. Jimenez, R. Saunders, and P. Brunel, 2010: A Tool to Estimate Land Surface Emissivities in the Microwave (TELSEM) for use in numerical weather prediction schemes. Q. J. Royal Meteor. Soc. (in review).

Anderson, J. L., 2003: A local least squares framework for ensemble filtering. *Mon. Wea. Rev.*, **131**, 634-642.

Boukabara, S.-A., and F. Weng, 2008: Microwave emissivity over ocean in all-weather conditions: Validation using WINDSAT and Airborne GPS Dropsondes. *IEEE Trans. Geosci. Remote Sens.*, **46**, 376-384.

Deblonde, G., and S. J. English, 2000: Evaluation of the FASTEM-2 fast microwave oceanic surface emissivity model. In the *Proc. Tech. ITSC-XI*, Budapest, Hungary, Sept. 20-26, pp. 67-78.

Ellison, W. J., S. J. English, K. Lamkaouchi, A. Balana, E. Obligis, G. Deblonde, T. J. Hewison, P. Bauer, G. Kelly, and L. Eymard, 2003: A comparison of ocean emissivity models using the Advanced Microwave Sounding Unit, the Special Sensor Microwave Imager, the TRMM Microwave Imager, and airborne radiometer observations. *J. Geophys. Res.*, **108**, D21, 4663, doi: 10.1029/2002JD002313.

English, S., and T. Hewison, 1998: A fast generic millimeter-wave emissivity model, *Proceedings of the SPIE*, 3503, 288-300.

Liebe, H. J., 1989: MPM- An atmospheric millimeter wave propagation model. *Int. J. Infrared Millimeter Waves*, **10**, 631-650.

Liebe, H. J., P. W. Rosenkranz, and G. A. Hufford, 1992: Atmospheric 60 GHz oxygen spectrum: New laboratory measurements and line parameters. *J. Quant. Spectros. Radiat. Transfer*, **48**, 629-643.

Liu, Q., and F. Weng, 2003: Retrieval of sea surface wind vectors from simulated satellite microwave polarimetric measurements. *Radio Sci.*, **38**, 8078-8085.

Kummerow, C., 1993: On the accuracy of the Eddington Approximation for radiative transfer in the microwave frequencies. *J. Geophys. Res. – Atmos.*, **98**, 2757-2765.

Olson, W. S., P. Bauer, C. D. Kummerow, Y. Hong, and W.-K. Tao, 2001: A melting layer-model for passive/active microwave remote sensing applications. Part II: Simulation of TRMM observations. *J. Appl. Meteor.*, **40**, 1164-1179.

Prigent, C., F. Aires, and W. B. Rossow, 2006: Land surface microwave emissivities over the globe for a decade. *Bull. Amer. Met. Soc.*, **87**, 1573-1584.

Wilheit, T. T., Jr., 1979: A model for the microwave emissivity of the ocean's surface as a function of wind speed. *IEEE Trans. Geosci. Electron.*, **GE-17**, 244-249.